Design criteria, fabrication, and application of high vacuum brazing furnace

Hardik A. Patel, Sunil Jha, Sudarshan Ghosh
Indian Institute of Technology, Delhi, India

Abstract

The recent demand for development in micro-diamond dressers has gained tremendous importance in the grinding industries. To successfully develop diamond dresser, it requires joining diamond grits to carbide surface firmly. The braze alloy with active element is used to join the diamond. The active braze alloy forms the stable oxides prior to reaching brazing temperature, that will diminish the bonding characteristics of the braze alloy. To prevent such transformation, the brazing is carried out in a high vacuum environment.

In the present article, the design criteria for the development of the vacuum chamber, selection of the vacuum pumping system, selection of resistance heating element, FE-modelling and simulation of single-layered and multi-layered radiation shield, and integration of the high vacuum furnace are described in detail. The results show the time required to achieve the 10^{-5} Torr is less than 2000 seconds. At ~ 1400 °C core temperature, the outermost body temperature of the single-layer and multi-layer radiation shield vacuum chamber is ~ 413.9 °C and ~ 40.4 °C, respectively. That is approximately ~ 921.97 % lower temperature in multi-layer compared to single-layer radiation shield. After final assembly, at 1100 °C the actual measured outer body temperature is 42 ˚C, near to the simulated multi-layered radiation shield of 40.2 °C; hence no water cooling /jackets are required. The diamond dresser is developed and analysed at the application stage under single grit scratch analysis. The SEM micrographs show no bond failures or grit pull-out under different experimental conditions. The maximum force that can withstand by the diamond dresser is 17.84 N and 8.27 N normal and tangential, respectively. The outcome of this investigation will be of immense interest to high vacuum furnace manufacturing industries associated with the development of brazed diamond grinding tools.

1 Introduction

A vacuum furnace is an essential tool in most research laboratories, particularly in developing new material and process, heat treatment, vacuum sintering, vacuum brazing, high-quality RF systems, and UHV components of high energy accelerators, and many more. The primary purpose of a vacuum furnace is to prevent the complication of oxidation during the thermal cycle. There are several laboratory-scale vacuum furnaces proposed for different applications.

Different researchers have conducted different studies to develop different types of vacuum furnaces for various applications. In vacuum brazing instead of single layer insulator, multilayer insulation gives more temperature drop due to radiation shielding effect [1-3]. Jianxiu Zhang et al. [4] has developed the thermal annealing furnace used in vacuum and different air environments to study the temperature/stress distribution and airflow vectors in the furnace. Gang Yang et al. [5] developed the simplified expression for charge and discharge convection heat transfer model by considering the rate of change of pressure dp/dt in the vacuum chamber. Qijiang Shu et al. [6] presented an effective method for an accurate temperature of the substrate surface by measuring the deviation between vacuum furnace temperature and material growth temperature based on the temperature measurement principle-controlled methods used in a vacuum furnace. Niedziela et al. [7] described the design, control, and characterization of a radiant heating vacuum furnace for the inelastic neutron scattering experiments.

In the present article, the design criteria for the development of the vacuum chamber, selection of the vacuum pumping system, selection of resistance heating element, FE-modelling and simulation of single-layered and multi-layered radiation shield, and integration of the high vacuum furnace are described in detail. Furthermore, the Diamond dresser is developed and experimental analysis has been carried out using single grit grinding scratch teste.

2 Design criteria

A vacuum brazing furnace is a combination of different components and sensors. The design of a vacuum brazing furnace is carried out in two individual steps: a) design and fabrication of chamber and selection of pumping system. And b) design and fabrication of furnace module.

2.1 Design and fabrication of chamber and vacuum pumping system

The vacuum chamber's design and material must have good mechanical strength, low intrinsic vapor pressure, low desorption rate, high gas tightness (vacuum related properties), high melting point, good thermal shock resistance, and low thermal expansion (temperature-related properties) at ambient temperature and vacuum condition. Focusing on the application, brazing of diamonds, the operating range of a brazing temperature is 650 ˚C to 1100 ˚C

with a vacuum level maintained below 10^{-5} mbar. [8-9], the low carbon variant of stainless steel "AISI 304L" is selected. Due to low carbon, it is easy to weld, and intergranular corrosion is very less.

The design of the chamber is made small to reduce the surface area and volume of the chamber. Cylindrical geometry is selected to reduce volume, surface area, and weld connection. According to ASME-VIII, Div-I, UG-28, [10] the thickness of the shell is calculated using allowable external pressure or shell under compression load is computed using the following formula:

$$P_{a1} = \frac{4AE}{3\left(\frac{D_0}{t}\right)} \quad (1) \qquad P_{a2} = \frac{4B}{3\left(\frac{D_0}{t}\right)} \quad (2)$$

P_{a1}, P_{a2} = maximum allowable external working pressure for the assumed value of t; D_o = outer diameter of the shell; t = thickness of the shell.
Factor "A" is selected from ASME Code, Section II, Part D, subpart 3 using figure G [11] for Do/t > 10, and factor "B" is selected from figure HA-3 Factor A falls to the left of the material line use equation 1 is considered and/or if factor A falling on the material line equation 2 is considered. 'The CAD of the chamber is shown in Figure 1 (a).'

The vacuum pump system is selected considering volume, the surface area inside a chamber assembly, vacuum level required, and approximate time to reach the vacuum level. To achieve vacuum level < 10^{-5} Torr, in the clean room environment, a turbomolecular pump is the best choice. The turbomolecular pump's application range is 10^{-1} Torr to 10^{-9} Torr; to achieve <10^{-1} Torr rotary vane pump is attached as a backing pump. The average pump-down time required to achieve the desired vacuum is calculated using the following formula. Pump downtime using a backing pump is calculated using eq. 3, followed by Pump downtime using a turbomolecular pump is calculated using eq. 4.

$$t_1 = \frac{v}{s}\ln\frac{p_0}{p_1} \quad (3) \qquad t_2 = \frac{v}{s_{turbo}}\ln\frac{p_1}{p_2} \quad (4)$$

t_1= pump-down time of backing pump, v = volume of vessel, s = pumping speed of backing pump, P_0 = Initial pressure, P_1 = intermediate pressure before starting turbopump <10^{-1} Torr; S_{turbo} = pumping speed of backing pump, P_1 = initial pressure after t_1, P_2 = Final pressure [12].

2.2 Design and fabrication of furnace module

Different materials are used in the furnace as heating elements such as, molybdenum, tantalum, graphite, and many more. Among all, high-density graphite material is the superior choice due to lightweight, easily machined to the required shape, become stiffer and stronger with increasing temperature, furthermore, high thermal shock resistance capacity allows the higher heating rate, and low spattering yield [5-6]. These characteristics of the graphite heating element attract high temperatures and long-life operation. 'A computer-

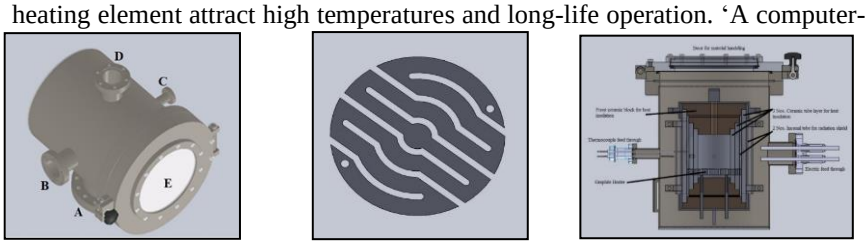

Figure 1. CAD of a) chamber, b) graphite heater, c) furnace assembly

aided design of pseudo-coil pattern shown in Figure 1 (b).' It is designed according to furnace chamber size. Design is made in such a manner to increase the appropriate resistance to achieve the desired temperature at low power and simple to machine. Considering the constant cross-section of the coil, pseudo-coil is modelled as a homogeneous graphite bar of total length L, thickness t, and width w. Hence, the resistor of resistance R_{pc} is calculated using equation 5:

$$P_{heater} = \frac{V^2}{R_{\rho c}(T)} \qquad (5) \qquad R_{\rho c} = \frac{\rho(T)L}{t\,w} \qquad (6)$$

where ρ(T) is the resistivity of graphite as a function of temperature. The heater power P_{heater} delivered at a given temperature and supply voltage is obtained using eq. 6. 'The final assembly CAD of the furnace module is shown in Figure 1 (c).'

2.3 FE-Modeling of radiation shields

Heat insulation for the vacuum furnace is selected carefully because gas entrapped by insulation and desorption rate of the material may take more time to achieve a high vacuum level and reduce the vacuum level at elevated temperatures. High-density pure alumina polished tubes having gas-tight strength, low emissivity, low thermal conductivity, and low thermal mass at elevated temperature properties are used as furnace radiation shield [1]. Initially, the heat shield insulation thickness is calculated by making a resistance circuit considering steady-state radiation and conduction problem. Finally, the temperature drops over the thickness is solved by making finite element model.

FE model and simulation of a furnace module with vacuum chamber with graphite heater is carried out considering transient conduction and radiation formula. A heating element is energised by transient heat flux input. The 3D furnace model is converted to 2D axisymmetric geometry model fig 4. Abaqus v6.19 software is used to simulate the model and vacuum body temperature is analysed under two condition. The temperature distribution in different radiation shield surface is also obtained. This temperature distribution is used to predict the insulation thickness to design the air-cooled furnace system.

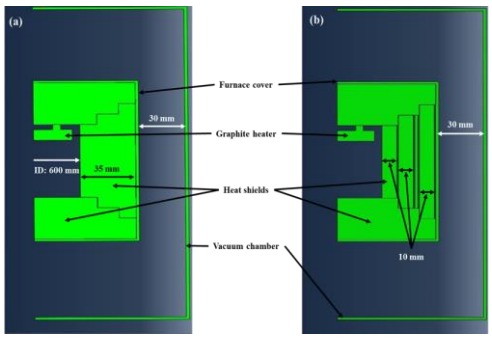

Figure 2. FE model a) single layer, b) multi-layer composite wall heat shield

The following assumptions/boundary conditions are considered in the FE-model. The conduction heat losses due to electrical leads are ignored. The heat radiation input to heat shield from the heater's surface is considered. Interaction

property between different surfaces includes the shape factor and emissivity of the independent material. The initial temperature of all nodes of the mesh elements of the furnace and a chamber is 25 °C.

The FE analysis is carried out for two different cases: a) single layer composite-wall insulation and b) multilayer composite-wall insulation.

(a) Single layer composite-wall heat shield is the combination of alumina tube ID: 60 cm and radial thickness 35 mm. The top and bottom heat shield thickness is 35 mm. The assembly is covered by a 2 mm Inconel-718 tube to maintain a clean vacuum environment. The outer body is a vacuum chamber made of SS304L 'Figure 2 (a)-shows the FE-model of single-layer composite wall heat shield.'

(b) Multilayer composite-wall heat shields consist of five different concentric insulators are used, separated by 1 mm radial clearance. Three nos. alumina insulator, 10 mm radial thickness, and two nos. Inconel-718 insulator, 2 mm radial thickness are used for radiation shield and to maintain a clean vacuum environment. The outer body is a vacuum chamber made of SS304L 'Figure 2 (b)-shows the FE-model of multi-layer composite wall heat shield.' The simulated temperature profile contour of single layer and multilayer composite wall heat shield are shown in Figure 3 (a and b)**,** respectively. The material property of different elements used to develop a furnace is shown in table 1.

Table 1. Material properties of the different components

Property	Graphite Heater [13]	Alumina [14]	Inconal718 (Insulation shield) [15]	SS304L chamber body [16]
Density/kg·m^{-3}	1.3	3.52	8.2	8.0
Sp. Heat/J·kg^{-1} K^{-1}	750	775	362	510
CTE/K^{-1}	5×10^{-6}	8.3×10^{-6}	1.3×10^{-5}	1.87×10^{-5}
Emissivity/W·m^{-1}	0.9	0.2	0.78	0.44
Th. Conductivity/W·m^{-1} K^{-1}	130	25	10	16.2

3 Result and discussion

The result discussion is divided into two major parts a) implementation and b) FE simulation results and experimental results of the developed furnace.

3.1 Thickness of vacuum chamber

The calculation is carried out considering initial assumption Do = 205 mm and L = 250 mm, the thickness is varying from 0.5 mm to 2.5 mm, the measured factor A is falling on the material line. Hance, maximum allowable external working pressure is calculated using equation 2. The design is safe above the 1 mm thickness shell. According to ASME-VIII Div-I, UG-16 (B), the minimum thickness permitted for shells and heads holding components shall be 1.6 mm. assuming factor safety 1.5 times for holding four flange connection 2.5 mm thickness of the chamber shell is selected for manufacturing.

3.2 FE-simulation and experimental results

Figure 3 shows the simulated temperature profile contour in the different parts of the vacuum furnace of a) single-layer composite insulator and b) multilayer composite insulation. The temperature drop in the multilayer insulation furnace is more than a single layer insulator due to radiation losses between the different insulation layers.

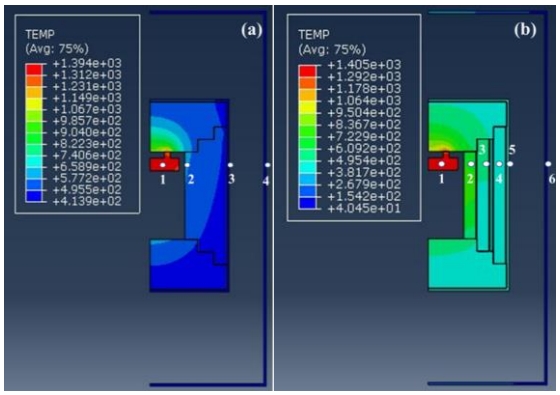

Figure 3. FE simulation of a) single layer, b) multi-layer composite wall heat shield

From the simulated result it is observed that the while graphite heater is heated to 1400 °C the vacuum chamber temperature is ~ 413.9 °C in case of single layered heat shield composite wall (Figure 3 a) and ~ 40.45 °C in case of the multi-layered heat shield composite-wall (Figure 3 b). i.e., ~ 921.97 % temperature drop in multi-layer heat shield compared to single-layer heat shield. The reason behind such drop is the 1 mm radial clearance between the five concentric heat shields. Figure 5 (b) - shows the actual temperature measured using a K-type thermocouple (Experimental) with the simulated temperature at the outer body of the vacuum chamber. There is not much temperature difference between the actual measured temperature and the simulated multi-layered temperature at outer chamber body.

The temperature difference between multilayer insulation and actual measured temperature is 40.5 °C and 52 °C, respectively. The experiment is conducted to measure the power vs. temperature of the developed vacuum furnace shown in figure 4. Figure 5 (a) - illustrate the actual time required to reach 10^{-5} Torr. Figure 5 (c) - shows the power curve for a heating rate of 10 °C/min and 20 °C/min. The power graph having an initial deviation, it is due to deviation between programmed temperature and actual temperature up to 100 °C - 150 °C. At the starting of the furnace graphite heater requires more power for the autotuning with a programmed temperature. The maximum power requires to achieve 1000 °C is with a different heating rate of 10 °C/min and 20 °C/min is < 950 W.

Figure 4. Assembly of vacuum brazing furnace

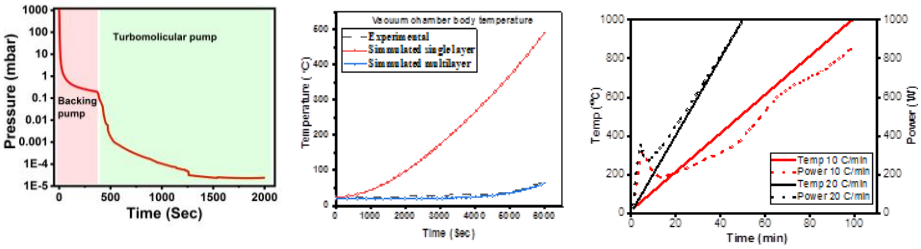

Figure 5. a) Time required to reach 10^{-5} Torr, b) Outer body temperature of experimental vs simulated single layer, and multi-layer composite wall, and c) actual power required to reach 1000 °C

4 Application

The overall performance of the grinding wheel is difficult to analyse, as it is a compilation of individual abrasive grit contribution. The single grit scratch test is useful to investigate the effect of the individual grit effect on the work material [17]. The diamond dresser is fabricated using the vacuum brazing furnace by joining of natural diamond grit of 0.5 mm

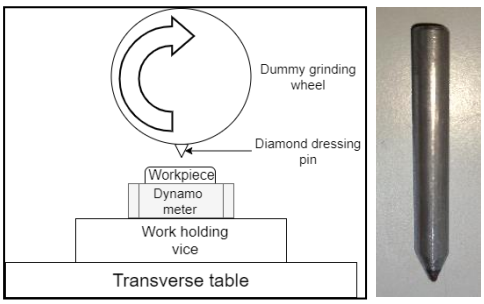

Figure 6. a) Schematics of the single grit scratch, b) Fabricated diamond dresser

onto mild steel pin the commercially available active brazing alloy. The brazing temperature is 950 °C for the dwell time of 15 minutes and the vacuum level is maintained $<10^{-5}$ Torr throughout the brazing cycle.

Bonding strength of brazed diamond dresser tool in terms of tangential and normal force was analysed using single scratch grinding experiment. Chevalier B818-III surface grinder was used for the single scratch grinding experiments. The forces are measured using Kistler dynamometer 9257B. 'The grinding schematics, fabricated diamond dresser is illustrated in Figure 6 (a and b).' The single grit scratch has been carried out at wheel speed 16 m/sec, table speed 4, 6, and 8 m/min, at 5, 10, and 15 µm depth of cut.

4.1 Experimental validation through single grit scratch teste

The measured normal and tangential forces for the single grit scratch condition at are shown in Figure 7 (a). It indicates that the developed single point diamond dresser can withstand maximum 17.84 N and 8.27 N normal and tangential force, respectively without grit failure.

After 9 different scratch experiment the diamond dresser is examined under scanning electron microscopy for the grit failure of bond failure. The grinding speed of 16 m/sec at lower depth of cut the diamond grits may sliding over the zirconia workpiece surface, the abrasion wear take place on the tip of the diamond grit, that increases the temperature in the grinding zone tremendously. The abrasive wear sets rapidly increase with increasing in depth of cut. Frictional rubbing of these wear flats in the scratch zone increases the temperature at the grit tip. Due to multiple scratch on the zirconia ceramic high thermal stress zone is created at the tip of diamond dresser. The combined abrasion and thermal stress zone start the microcracking of the diamond grits at the tip. 'SEM image of the tool after the experiment is shown in Figure 7 (b).' Which clearly indicates that the diamond grit wears out due to the microcracking effect.

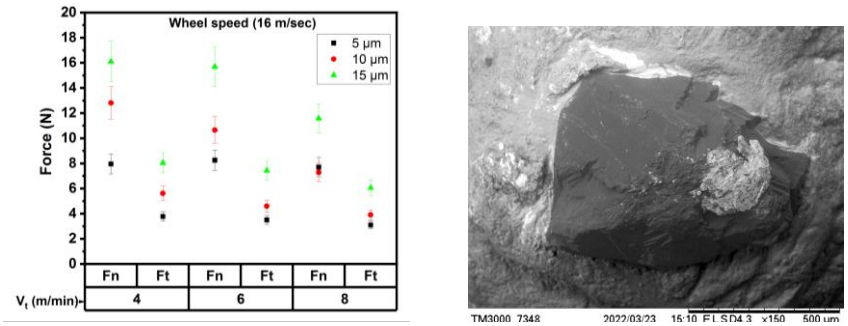

Figure 7. a) Normal and tangential force under different scratch condition, and b) SEM micrograph of the diamond dresser after single grit scratch

4 Conclusion

This article explains the design and development steps of high vacuum furnace with an electric resistance heater for the brazing application.

- The vacuum chamber design is carried out using ASME-VIII, Div-1, UG-16, and UG-28, considering material properties from ASME Code, Section II, Part D, and subpart 3 SS304L.
- The turbomolecular pump with a rotary vane pump as a backing pump combination is selected. The pump downtime to achieve < 10^{-5} Torr vacuum level in less than 2000 second. The calculated pump downtime varies with actual pump down time due to different surfaces having different desorption rates.
- A High-density graphite heater is selected for a heating element. And 99.9 % polished alumina tubes as selected for radiation shield. The FE-simulates result shows that the multi-layer composite wall heat shield temperature drop compared to a single-layer composite wall heat shield is more than 900% (921.97 %).
- The maximum power requires to achieve 1000 ˚C is < 950 W with a different heating rate of 10 and 20 ˚C/min.
- The outer body temperature is < 50 ˚C at an elevated temperature at 1000 ˚C. Hence, no water cooling and chiller unit are required.
- The tengential force and normal force 17.84 N and 8.27 N forces can withstand by the brazed tool without failure, the diamond grit wears out due to the microcracking effect only.

Acknowledgment

This work was supported by the Department of Science and Technology, Govt. of India. Under the project “Advanced CNC micromachining system with integrated micro tool manufacturing” [DST/TSG/NTS/2015/114-G, 2016].

References

[1] Cohen J, and Eaton W 1960 High temperature high vacuum resistance furnace *Rev. Sci. Instr.* 31 522
[2] Austerman S B 1961 Compact high-temperature vacuum furnace *Rev. Sci. Instr.* 32 8 522
[3] Kornelsen E V 1959 High-temperature laboratory vacuum furnace *Rev. Sci. Instr.* 30 290
[4] Jianxiu Zhang, Zhongjun Tian, and Kunpeng Wang 2020 Optimal design of the annealing furnace and quality improvement for KDP crystals *Optik - International Journal for Light and Electron Optics* 217 164874
[5] Gang Yang, Linglong Du, Jingmin Du, Baoren Li and Xiaoyun Fu 2017 Convection heat transfer model and verification for the vacuum chamber during charge and discharge processes *Vacuum* 139 67-76

[6] Qijiang Shu, Jing Liu, Xu Lan, Jia Long, Jie Yang, Chong Wang and Yu Yang 2017 Correction analysis for the deviation between vacuum furnace and material growth temperatures *Vacuum* 144 21-26
[7] Niedziela J L, Mills R and Loguillo M J 2017 Design and operating characteristic of a vacuum furnace for time-of-flight inelastic neutron scattering measurements *Rev. Sci. Instrum*. 88, 105116
[8] Jinbin Lua, Ziyang Cao, Fangjuan Qia, Mi Qiana and Wangxi Zhang 2018 Evolution of interface carbide diamond brazed with filler alloy containing Cr *Diamond & Related Materials* 90 116–125
[9] Sixing Liu, Bing Xiao, Haozhong Xiao, Longhui Meng, Ziyu Zhang and Hengheng Wu 2016 Characteristics of Al2O3/diamond/c-BN/SiC grain steel brazing joints using Cu–Sn–Ti active filler powder alloys *Surface & Coatings Technology* 286 376–38.
[10] ASME Boiler and pressure vessel code, Section VII-Division 1 2019 rules for construction of pressure vessels
[11] ASME Boiler and pressure vessel code, section II- part D 2015 material properties,
[12] Pfeiffer vacuum GMBH, The vacuum technology book, Volume II, Part 2: Know-how book, https://www.pfeiffer-vacuum.com/en/download-center/
[13] Entegris 2013 Properties and Characteristics of Graphite
[14] Auerkari 1996 Mechanical and physical properties of engineering alumina ceramics, VTT manufacturing technology, *Technical research center of Finland and Espoo*
[15] Díaz-Álvarez J, Cantero J L, Miguélez H and Soldani X 2014 Numerical analysis of thermo-mechanical phenomena influencing tool wear in finishing turning of Inconel718 *International Journal of Mechanical Sciences* 82 161–169.
[16] Choong S. Kim 1975 Thermophysical properties of stainless steels *Argonne national laboratory*, *Iilinois* 60439
[17] Anand P, Arunachalam N and Vijayaraghavan L 2019 Evaluation of grinding strategy for bioceramic material through a single grit scratch test using force and acoustic emission signals. J*ournal of Manufacturing Processes* 37 457–469